IMMUNOLOGY

STING couples with PI3K to regulate actin reorganization during BCR activation

Yukai Jing[1,2]*, Xin Dai[1]*, Lu Yang[1]*, Danqing Kang[1], Panpan Jiang[1], Na Li[3], Jiali Cheng[1], Jingwen Li[1], Heather Miller[4], Boxu Ren[3,5], Quan Gong[3,5], Wei Yin[6], Zheng Liu[7], Pieta K. Mattila[8], Qin Ning[9], Jinqiao Sun[10], Bing Yu[1†], Chaohong Liu[1†]

The adaptor protein, STING (stimulator of interferon genes), has been rarely studied in adaptive immunity. We used *Sting* KO mice and a patient's mutated *STING* cells to study the effect of STING deficiency on B cell development, differentiation, and BCR signaling. We found that STING deficiency promotes the differentiation of marginal zone B cells. STING is involved in BCR activation and negatively regulates the activation of CD19 and Btk but positively regulates the activation of SHIP. The activation of WASP and accumulation of F-actin were enhanced in *Sting* KO B cells upon BCR stimulation. Mechanistically, STING uses PI3K mediated by the CD19-Btk axis as a central hub for controlling the actin remodeling that, in turn, offers feedback to BCR signaling. Overall, our study provides a mechanism of how STING regulates BCR signaling via feedback from actin reorganization, which contributes to positive regulation of STING on the humoral immune response.

INTRODUCTION

STING (stimulator of interferon genes; also called MITA, MPYS, or ERIS) is expressed in hematopoietic cells in peripheral lymphoid tissues and is also highly expressed in nonlymphoid tissues, such as the lung and heart. STING locates to the endoplasmic reticulum (ER) and mitochondria-associated ER membrane (*1*). STING interacts with interferon regulatory factor 3 (IRF3) to activate the type I interferon production in response to foreign DNA from a variety of intracellular pathogens (*2*, *3*). STING has also been reported to be involved in the pathogenesis of systemic lupus erythematosus (SLE) (*4*–*7*). The expression of STING is low in patients with SLE and in MRL/lpr mice, of which the MRL/lpr mice have higher expression of JAK1 (Janus kinase 1) and lower expression of tyrosine phosphotases, SHP1 and SHP2 (*8*). Furthermore, SLE B cells have highly activated B cell receptor (BCR)–, Toll-like receptor 7 (TLR7)–, and TLR9-mediated signaling pathways that are involved in reducing STING expression (*8*). The link between STING and lupus demonstrates the importance of determining the regulation of STING on BCR signaling.

Phosphatidylinositol 3-kinase (PI3K) is important for the development and differentiation of B cells, and the class I PI3K consists of a catalytic subunit p110 and a regulatory subunit p85 (*9*). Splenic marginal zone (MZ) B cells and B1a cells are significantly reduced in p110δ-deficient mice (*10*). In B cells, the majority of cytosolic PI3K is associated with the membrane adaptor protein CD19, which effectively recruits p85α via tandem YXXM motifs (*11*). Mice with B cell–specific deletion of PTEN have elevated PI3K signaling, as well as increased MZ B cells and B1a cells (*12*). The absence of PTEN and the consequential increase in PI-3,4-P2 and PI-3,4,5-P3 can substitute the role of CD19 in promoting PI3K activity (*12*), and a similar function is also exhibited by another inositol phosphatase, SHIP. Lyn phosphorylates CD19, which in turn recruits PI3Ks. Lyn activation also stimulates the activation of Vav which contributes to PI3K activation in B cells by activating Rac1, which binds to PI3Ks via its Rho guanosine triphosphatase activating protein (RhoGAP) domain (*13*, *14*). PI3K/PIP_3 signaling then turns on Akt signaling via Akt/PDK-1 activation and reduces apoptosis by phosphorylating Foxo-1/3 and promoting their nuclear export and degradation (*15*, *16*). PIP_3 binds PDK1 and PDK1 phosphorylates Akt, which activates mTORC1 directly or indirectly through the actions of TSC1/TSC2 (*17*, *18*). STING has been shown to regulate the tyrosine phosphatase, SHP (*8*), but whether it can regulate SHIP during BCR activation still remains elusive.

BCR activation is vital for the function of B cells, such as the formation of germinal centers (GCs), isotype switching, and somatic hypermutation. The initiation of BCR activation starts with the binding of antigen to the BCR, which is thought to induce BCR clustering by cross-linking BCRs. The conformational change of the BCR exposes the activation site and recruits Lyn to phosphorylate the ITAM (immunoreceptor tyrosine-based activation motif) domains of the Igα and Igβ sheets of the BCR complex. The recruitment and activation of Syk leads to the activation of Btk, phospholiphase Cγ (PLCγ), and downstream signaling molecules. Our previous research has shown that BCR activation leads to actin reorganization, which offers feedback to the BCR signaling by modulating the spatiotemporal organization of BCRs (*19*–*21*). Btk activity leads to the activation of Wiskott-Aldrich syndrome protein (WASP), an actin nucleation factor, by regulating the activity of Vav, the generation of PtdIns-4,5-P2, and the direct phosphorylation of WASP (*22*). Whether STING regulates BCR signaling to orchestrate actin reorganization is unknown.

In our study, we used *Sting* knockout (KO) mice to examine the effect of STING deficiency on BCR signaling and actin reorganization.

[1]Department of Pathogen Biology, Tongji Medical College, Huazhong University of Science and Technology, Wuhan, China. [2]Department of Medical Laboratory, The Central Hospital of Wuhan, Tongji Medical College, Huazhong University of Science and Technology, Wuhan, China. [3]Department of Immunology, School of Medicine, Yangtze University, Jingzhou, China. [4]Department of Intracellular Pathogens, National Institute of Allergy and Infectious Diseases, Hamilton, MT 59840, USA. [5]Clinical Molecular Immunology Center, School of Medicine, Yangtze University, Jingzhou, China. [6]Wuhan Children's Hospital, Tongji Medical College, Huazhong University of Science and Technology, Wuhan, China. [7]Department of Otolaryngology-Head and Neck Surgery, Tongji Hospital, Tongji Medical College, Huazhong University of Science and Technology, Wuhan, China. [8]Institute of Biomedicine, Unit of Pathology, and MediCity Research Laboratories, University of Turku, Turku, Finland. [9]Department of Infectious Disease, Tongji Hospital, Tongji Medical College, Huazhong University of Science and Technology, Wuhan, China. [10]Department of Clinical Immunology, Children's Hospital of Fudan University, Shanghai, China.
*These authors contributed equally to this work.
†Corresponding author. Email: yubing@hust.edu.cn (B.Y.); chaohongliu80@126.com (C.L.)

We found that the activation of the proximal positive BCR signaling molecule, CD19, and downstream molecule, Btk, was enhanced and that the proximal negative BCR signaling molecule, SHIP, was decreased in *Sting* KO B cells after BCR stimulation. The distal BCR signaling of PI3K-mediated Akt and mTORC1 activation was also up-regulated as well as the phosphorylation of WASP and resultant actin reorganization. By using total internal reflection fluorescence microscopy (TIRFm), we found that the BCR clustering was reduced, but B cell spreading was increased in *Sting* KO B cells after stimulation with membrane-associated antigens. The inhibition of PI3K rescued the defect of BCR clustering, B cell spreading, actin reorganization, and BCR signaling. Overall, our study provides a new regulatory pathway of BCR signaling based on the negative regulation of STING on the PI3K central hub and regulation of actin reorganization via WASP.

RESULTS

The deficiency of STING alters the homeostasis of peripheral B cells but not the developmental subsets in the bone marrow

To determine whether STING affects the development of bone marrow (BM) B cells, we stained the different subpopulations of BM B cells with BP1 and CD24 antibodies to distinguish pre-pro, pro, and early-pre; and B220-IgM antibodies to separate late-pre, immature, and recirculating B cells. We did not observe any changes for most of the subpopulations except for decreased percentages and numbers of recirculating B cells in *Sting* KO mice (Fig. 1A and fig. S1, A and B). We further examined the interleukin-7 receptor (IL-7R) (CD127) expression that is crucial for the early development of BM B cells, and not surprisingly, we did not observe altered levels of CD127 in the STING-deficient mice (Fig. 1B). Therefore, STING is dispensable for the development of B cells in the BM. We further examined the deficiency of STING on the differentiation of peripheral B cells. We used immunoglobulin M (IgM)–IgD antibodies to stain the transitional 1 (T1), T2, and follicular (FO) B cells, CD21-CD23 antibodies to stain the MZ B cells, and CD95-GL7 antibodies to stain the GC B cells. We found that the percentage and number of MZ and GC B cells were significantly increased in *Sting* KO mice, but that of FO, T1, and T2 showed no changes (Fig. 1, C to G and fig. S1, C to E). To further confirm that the increase in MZ and GC B cells in *Sting* KO mice is cell intrinsic, a 1:1 ratio of CD45.1 wild-type (WT) with CD45.2 WT or *Sting* KO BM B cells was injected into CD45.1-recipient mice to generate chimera mice. Similarly, we found that the percentage of CD45.2 *Sting* KO MZ and GC B cells was increased compared with CD45.2 WT MZ and GC B cells after reconstitution (fig. S1, F and G). We also did not find any difference for the proliferation and apoptosis of each peripheral subpopulation (fig. S2). Next, we examined the effect of STING deficiency on the development and differentiation of T cell lineages. We found that the percentage and number of $CD4^+$, $CD8^+$, and $CD4^+CD8^+$ T cells were not altered in the thymus, spleen, and lymph node (LN) of *Sting* KO mice (fig. S3, A to G). Furthermore, we found that the percentage and number of regulatory T cells (T_{regs}) and cytokine production T cells including interferon-γ (IFN-γ), IL-4, and IL-17A were also the same in the thymus, spleen, and LN between WT and *Sting* KO mice (figs. S3, H to J and S4, A to H). Furthermore, we examined the architecture of the spleen of WT and *Sting* KO mice with hematoxylin and eosin (H&E) staining and immunofluorescence, which showed correlation with the increased GC B cells in *Sting* KO mice. We found an enlarged and darker staining of follicular area and larger sizes of $GL7^+$ GCs in *Sting* KO spleens compared with that of WT (Fig. 1, H to K). These results indicate that STING suppresses the differentiation of MZ and GC B cells. Last, we examined the peripheral blood mononuclear cell (PBMC) from a *STING* mutant patient, and we did not observe any changes for the frequency of transitional B cells and plasmablast cells (PBCs) (fig. S4I). But the percentage of unswitched and memory B cells (MBCs) was decreased, and that of naïve B cells was increased in *STING* mutant patient compared with that of the healthy control (HC) (fig. S4J).

STING is involved in BCR activation

Since we found that STING is involved in the homeostasis of peripheral B cells, which is largely determined by BCR signaling (*23*–*25*), we next examined the involvement of STING in BCR activation by confocal microscopy. WT splenic B cells were stimulated with soluble antigens (sAg) for varying lengths of time and then stained with antibodies specific for STING. The spatiotemporal relationship between BCR and STING was determined by the correlation coefficient to indicate the colocalization between BCR and STING. We found that the correlation coefficient increased gradually up to 10 min and dropped afterward (Fig. 2, A and B). Because the *Sting* KO is a germline deletion, we examined STING expression in splenic B cells of *Sting* KO mice. We did not detect STING expression in KO B cells by immunoblot (Fig. 2C). Considering STING is located at the ER, we examined whether the dynamics of the ER was altered in *Sting* KO B cells upon antigenic stimulation by using ER-Tracker dyes. The staining pattern of the ER was the same for *Sting* KO B cells and WT B cells, as well as the colocalization of ER with BCR (Fig. 2, D and E). To investigate how STING colocalizes with the BCR on the surface, we examined the distribution of ER or STING with BCRs by three-dimensional microscopy. We found that both ER and STING colocalized with the BCR cap at 10 min upon antigenic stimulation, which indicates they moved to the BCR cap together (fig. S5, A and B). Since SLE can cause an abnormal increase in MZ B cells and STING is linked to SLE (*7*, *26*–*28*), we examined the anti–double-stranded DNA (dsDNA) antibody levels in WT and KO mice by enzyme-linked immunosorbent assay (ELISA). We found an increase in anti-dsDNA antibody levels in *Sting* KO mice (Fig. 2F), and the glomeruli of the KO mouse kidney contained prominent IgG and complement deposits, which correlates with systemic autoimmunity that is frequently associated with renal pathology (Fig. 2, G and H). Because *Sting* KO mice develop autoimmunity with age, we measured the germinal center B cells (GCBCs) in aged mice and did not observe any difference for the percentage and number of GCBCs between aged WT and *Sting* KO mice, although the percentage and/or number of GCBCs both increased in aged WT and *Sting* KO mice (Fig. 2, I and J and fig. S1E). We found lymphocyte infiltration in the kidney, lung, and colon with high pathology scoring but not in the liver of *Sting* KO mice, and also the villi structure in the colon was completely destructed compared with that of WT mice (Fig. 2, K and L and fig. S5C). These results imply that STING is involved in B cell activation and controlling the peripheral tolerance of B cells.

STING deficiency up-regulates the proximal positive BCR signaling

Since STING is involved in the hyperactivation of B cells, we further investigated the effects of STING on BCR signaling. Btk-mediated

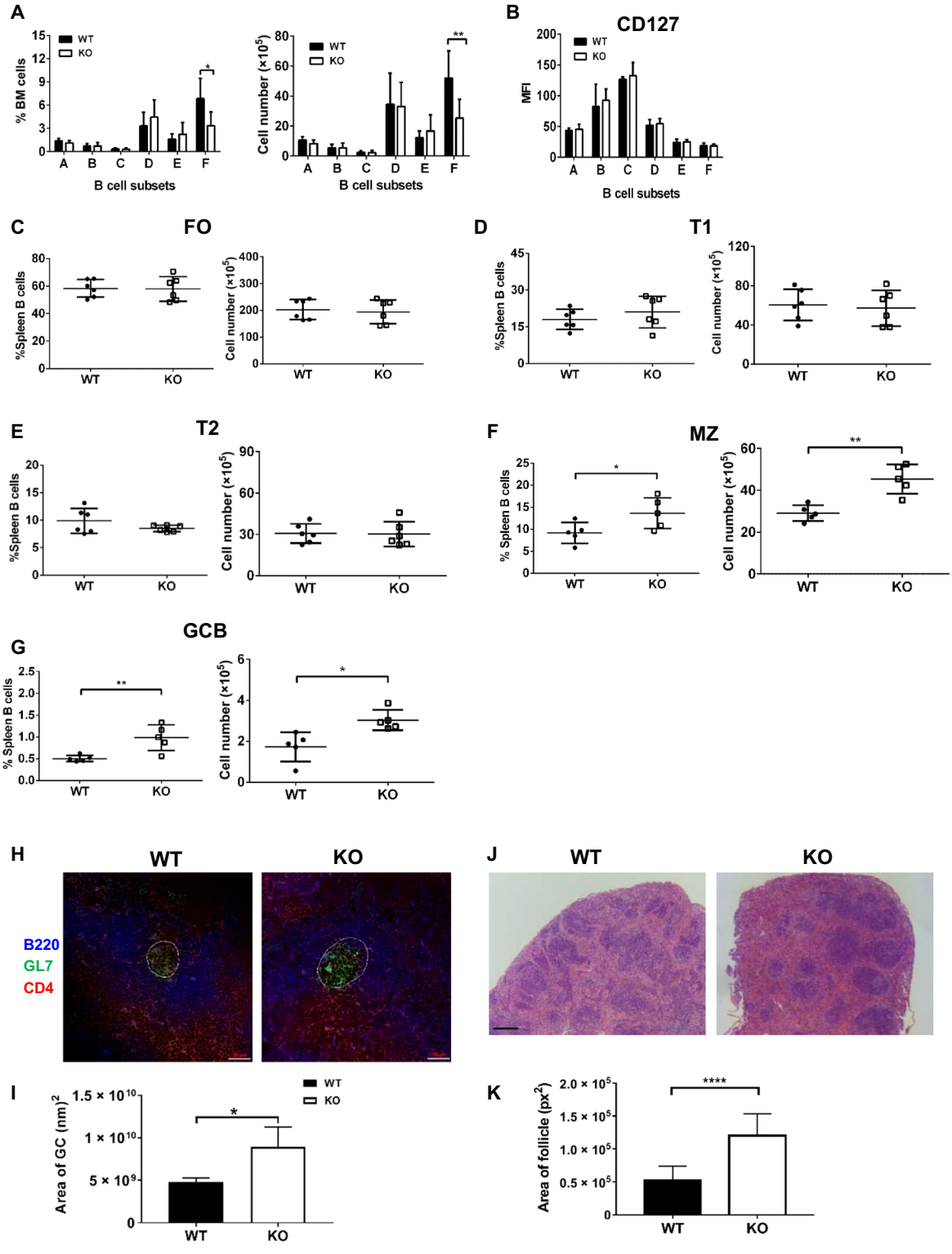

Fig. 1. STING deficiency impacts the differentiation of MZ and GC B cells, but not the development of BM B cells. Cells from BM of 6- to 8-week-old WT and *Sting* KO mice ($n = 6$) were labeled with Abs specific for surface markers of pre-pro (A), pro (B), early-pre (C), late-pre (D), immature (E), and recirculating mature B cells (F) and analyzed by flow cytometry. Shown are the average percentages (±SD) and numbers of total cells extracted from BM (**A**), and the average mean fluorescence intensity (MFI) of CD127 in B cell subsets (**B**). Splenic cells were stained with Abs specific for surface markers of T1, T2, FO ($n = 6$), MZ, and GC ($n = 5$) B cells. Samples were analyzed using flow cytometry. Shown are the average percentages (±SD) and numbers of subpopulations in spleen (**C** to **G**). Immunofluorescence staining of spleen sections from WT and *Sting* KO mice. Shown are representative follicles using pseudocolors: B220 (blue), CD4 (red), and GL7 (green); 20× objective; scale bars, 50 μm (**H**). H&E staining of spleen sections from 8-week-old WT and *Sting* KO mice. Scale bars, 200 μm (**J**). Quantification of the area of GCs and follicles from four mice (**I** and **K**). $^*P < 0.05$; $^{**}P < 0.01$; $^{****}P < 0.0001$.

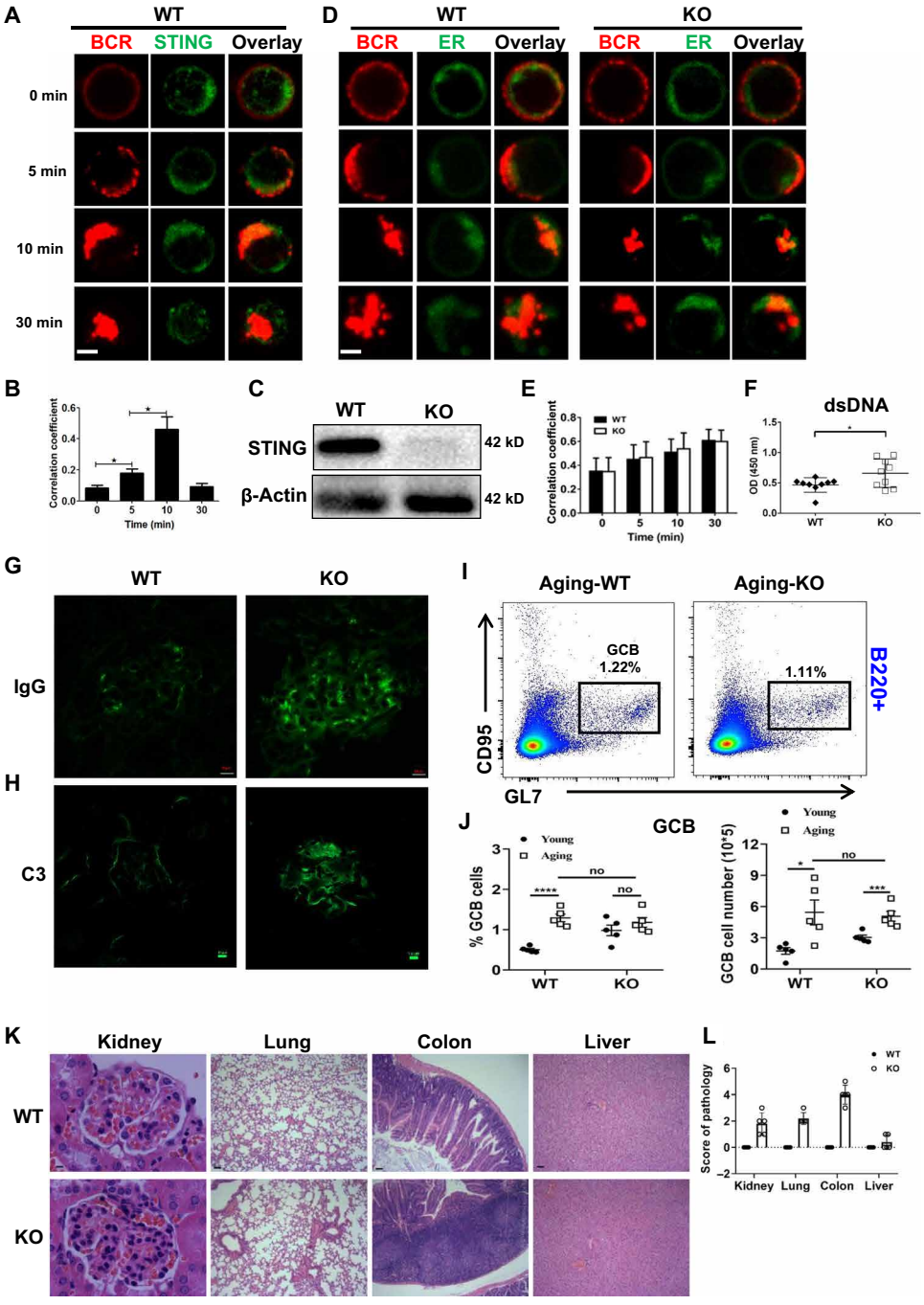

Fig. 2. STING is involved in BCR activation. Purified splenic B cells from WT and *Sting* KO mice were labeled with AF546-mB-Fab-anti-Ig and activated by incubating with either streptavidin or the medium alone (0 min) as a control at 37°C for varying lengths of time. After fixation and permeabilization, samples of WT were stained with antibodies for STING or ER-Tracker Blue-White DPX dye, and samples of KO were stained with ER-Tracker Blue-White DPX dye. Then, samples were analyzed using confocal microscopy. Shown are representative images (**A** and **D**) and the correlation coefficients between the labeled BCR and STING (**B**) or ER (**E**) quantified using the ZEN 2.3 (blue edition) software. Scale bars, 2.5 μm. Splenic B cells from WT and *Sting* KO mice were lysed, and then the lysates were probed with antibodies specific for STING (**C**). Enzyme-linked immunosorbent assay (ELISA) quantification of anti-dsDNA Ab in the serum of WT and *Sting* KO mice ($n = 9$). Dots represent individual mice (**F**). Immunofluorescence analysis of nephritic sections. Shown are representative glomeruli (**G** and **H**). 60× objective; scale bars, 25 μm. Flow cytometry analysis of GCB cells in spleens from aging (>5 months) and young (6- to 8-week-old) WT and *Sting* KO mice. Shown are representative dot plots of aging mice and the average percentages (±SD) and numbers of GCB cells in spleens of WT and *Sting* KO mice (**I** and **J**). H&E staining of kidney, lung, colon, and liver from WT and *Sting* KO mice. Shown are representative images and the pathological score from five mice (**K** and **L**). Each item was scored on a 5-point scale as follows: 0 = minimal damage, 1+ = mild damage, 2+ =moderate damage, 3+ =severe damage, and 4+ =maximal damage. For kidney, scale bar is 20 μm. For lung, colon, and liver, scale bars are 200 μm. *$P < 0.05$; ****$P < 0.0001$.

PI3K signaling is critical for the maintenance and differentiation of MZ B cells, so we investigated whether this signaling axis could be augmented in STING-deficient B cells. First, we examined the effect of STING deficiency on the spatiotemporal organization of phosphotyrosine proteins (pY), which represents the total levels of BCR signaling, and phosphorylated Btk (pBtk) by specific antibody staining using confocal microscopy. We found that the colocalization between pY/pBtk and BCRs was significantly increased in *Sting* KO B cells compared with that of WT B cells (Fig. 3, A and B). Furthermore, splenic B cells stimulated with sAg for varying lengths of time were lysed and probed with antibodies specific for pY, pSyk, Syk, pBtk, and Btk. We found that the levels of pY and the ratio of pSyk/Syk and pBtk/Btk were significantly enhanced in *Sting* KO B cells (Fig. 3, C to F). The increase in pY levels was recapitulated in the peripheral B cells of the *Sting* mutant patient (Fig. 3, G and H). CD19 is an upstream regulator of Btk during BCR activation, and similarly, we examined the spatiotemporal relationship between BCRs and pCD19 using confocal microscopy and activation levels of CD19 using immunoblotting. We found increased levels of pCD19 by immunoblot, as well as increased colocalization between BCR and pCD19 in *Sting* KO B cells (Fig. 3, I to L). To exclude the effect of STING deficiency on the expression of total CD19, we examined the expression levels of total CD19 in *Sting* KO B cells and did not observe any difference compared with that of WT B cells (Fig. 3M). All these results collectively suggest that STING negatively regulates BCR signaling by inhibiting the activation of CD19 and Btk.

STING deficiency down-regulates the activation of the negative BCR signaling molecule SHIP

Since the activation of Btk and SHIP counters each other, we examined the effect of STING deficiency on the spatiotemporal organization between pSHIP and BCRs as well as the activation levels of SHIP. Splenic B cells were activated with sAg for varying lengths of time and then stained with pSHIP-specific antibody for examination by confocal microscopy. We found that the correlation coefficient between BCR and pSHIP was significantly decreased in *Sting* KO B cells compared with that of WT B cells at 10 min (Fig. 4, A and B). Splenic B cells were also activated with sAg for varying lengths of time and then lysed and probed with antibody specific for pSHIP and SHIP for analysis by immunoblotting. We found that the ratio of pSHIP/SHIP was markedly decreased in *Sting* KO B cells at 5 min after activation, the time of peak intensity for pSHIP signal in WT cells (Fig. 4, C and D). Because SHP1 dephosphorylates Syk and Btk directly, we next examined the phosphorylation and total levels of SHP1. We did not observe any difference for the ratio of pSHP1/SHP1 between WT and KO B cells upon antigenic stimulation (Fig. 4, C and E). These results indicate that STING negatively regulates BCR signaling by enhancing the activation of SHIP.

STING deficiency causes an abnormal accumulation of F-actin via WASP

Our previous research has shown that Btk-mediated PI3K signaling modulates the accumulation of actin via WASP (*22*). So we investigated the effect of STING deficiency on actin reorganization. Splenic B cells were stimulated with sAg for varying lengths of time and then stained with phalloidin and anti-pWASP antibody for evaluation using confocal microscopy. We found that the correlation coefficient between pWASP and BCRs was significantly increased in *Sting* KO B cells at 0 and 10 min (Fig. 4, F and G). Furthermore, we examined the levels of pWASP and accumulation of F-actin using Phosflow. We found that the pWASP levels were significantly higher at 5 and 10 min in *Sting* KO B cells upon stimulation compared with that of WT B cells (Fig. 4H). The depolymerization phase of actin was attenuated in *Sting* KO B cells and caused an enhanced actin polymerization phase from 10 to 30 min (Fig. 4I). These results indicate that STING negatively regulates the actin polymerization via inhibiting the activation of WASP, likely via the Btk-PI3K signaling axis.

STING deficiency causes an abnormal accumulation of F-actin via PI3K-mediated signaling

To further confirm whether STING regulates actin reorganization via PI3K-mediated signaling, we used a PI3K-specific inhibitor, IC87114. To clearly observe the events occurring close to the membrane, we used TIRFm to observe the accumulation of BCR, BCR signaling molecules, and F-actin in the contact zone of B cells interacting with antigens tethered to lipid bilayers (mAgs). We used mAgs to stimulate splenic B cells pretreated with or without IC87114 for varying lengths of time and then stained the samples with pY-specific antibody and phalloidin. We found that BCR accumulation measured by mean fluorescence intensity (MFI) was significantly decreased in *Sting* KO B cells (Fig. 5, A, C, and E) and that the BCRs could not form the central BCR cluster, which corresponds to down-regulation of BCR signaling (*20*, *21*); instead, the KO displayed a punctate pattern (Fig. 5, A and C). However, the contact area of *Sting* KO B cells was significantly increased at very early time points, indicating faster and more efficient activation (Fig. 5, A, C, and F). The accumulation of pY and F-actin in the contact zone was also significantly enhanced in *Sting* KO B cells compared with WT B cells (Fig. 5, A, C, G, and H). WT B cells pretreated with PI3K inhibitor had significantly decreased BCR accumulation that was equal to the degree of that of KO B cells (Fig. 5, B, C, and E). In KO B cells treated with PI3K inhibitor, the BCR accumulation was restored close to the degree of WT B cells (Fig. 5, A, D, and E), and the contact area was almost restored to the level of WT B cells (Fig. 5, A, D, and F). For pY signaling, WT B cells treated with PI3K inhibitor had BCR signaling that was significantly decreased compared with that of untreated WT B cells (Fig. 5, A, B, and G). In KO B cells treated with PI3K inhibitor, the pY was partially restored (Fig. 5, D and G). For F-actin, WT B cells treated with PI3K inhibitor had their F-actin levels significantly decreased (Fig. 5, A, B, and H). In KO B cells treated with PI3K inhibitor, the levels of F-actin were reduced close to that of WT B cells (Fig. 5, A, D, and H). Furthermore, we investigated the effect of STING deficiency on the PI3K signaling as well as signaling molecules downstream of PI3K, Akt, and Foxo-1. The activation of Akt also leads to the initiation of mTORC1 signaling, so we examined the activation of pS6, which is the immediate downstream signaling molecule of mTORC1. Splenic B cells were activated with sAg, lysed, and probed with antibodies specific for pPI3K, PI3K, pAkt, Akt, pS6, S6, pFoxo-1, and Foxo-1. We found that the ratios of pPI3K/PI3K, pAkt/Akt, pFoxo-1/Foxo-1, and pS6/S6 were all clearly increased in *Sting* KO B cells (Fig. 5, I to N). The level of pPI3K was higher during the resting and activated states in the peripheral B cells of the *STING* mutant patient cells compared with that of the HC (Fig. 5, O and P). Since STING acts through the PI3K pathway, we investigated the direct effect of STING deficiency on PI3K recruitment and activity. First, we examined PI3K/pPI3K recruitment by confocal microscopy. We found

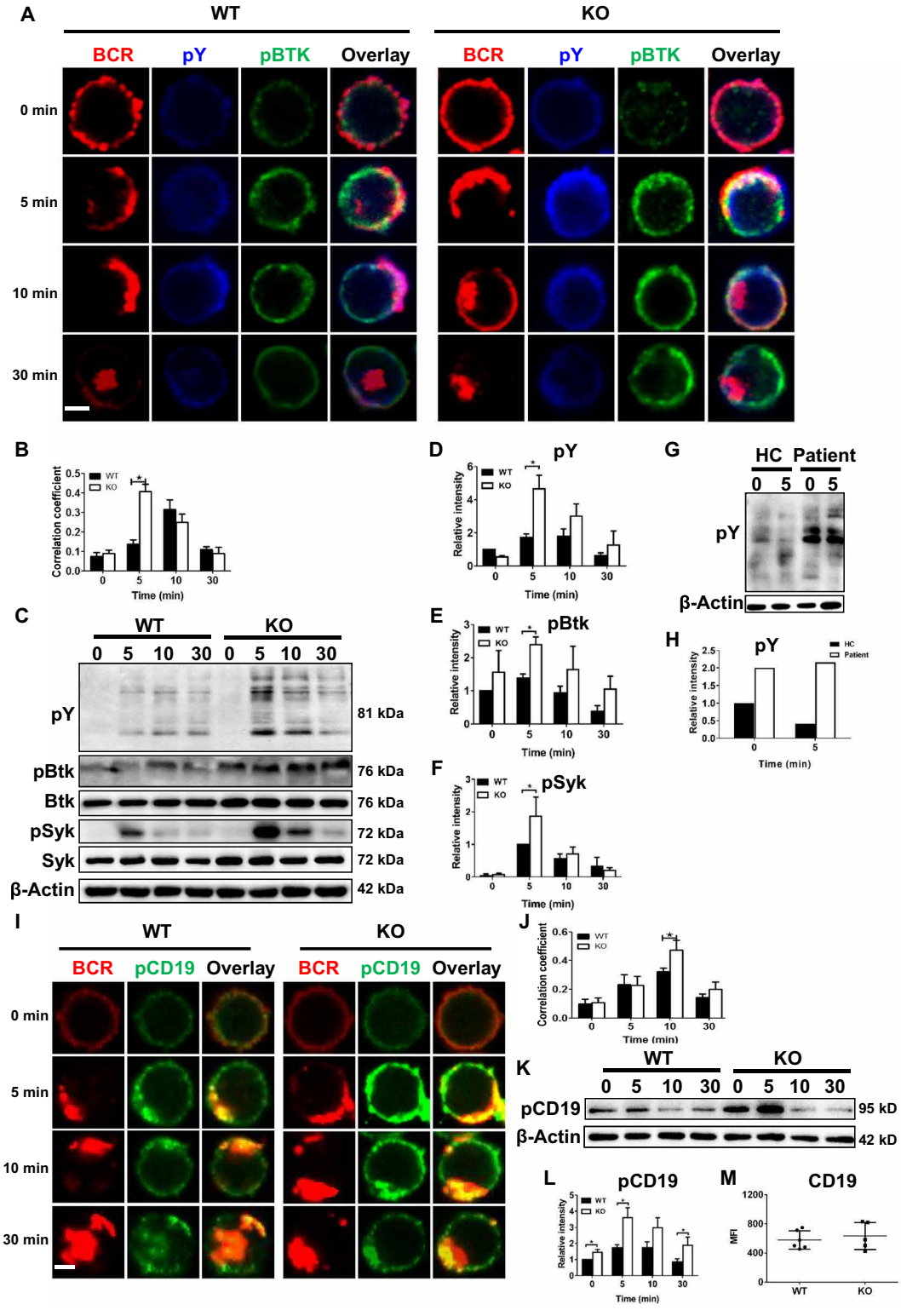

Fig. 3. STING deficiency up-regulates positive BCR signaling. Confocal analysis of splenic B cells from WT and KO mice labeled with AF546-mB-Fab–anti-Ig and then without or with streptavidin to activate. Cells were fixed, permeabilized, and stained with Abs specific for pY, pBtk (**A**), and pCD19 (**I**). Shown are representative images and the correlation coefficients between the labeled BCR and pY/pBtk (**B**) and pCD19 (**J**) from three independent experiments. Scale bars, 2.5 μm. Splenic B cells from WT and *Sting* KO mice were activated with biotin-conjugated F(ab')$_2$ anti-mouse Ig (M + G) plus streptavidin for indicated times. Cell lysates were analyzed using SDS–polyacrylamide gel electrophoresis (PAGE) and Western blot and probed for pY, pBtk, Btk, pSyk, Syk (**C**), and pCD19 (**K**). Total protein or β-actin as controls. Shown are representative blots of three independent experiments and blots' relative intensity (**D** to **F** and **L**). Western blot analysis of the level of pY in purified B cells from PBMCs of the healthy control and *STING* mutant patient (**G** and **H**). Flow cytometry analysis of MFI of CD19 in B220$^+$ B cells from WT and *Sting* KO mice (**M**). *$P < 0.05$.

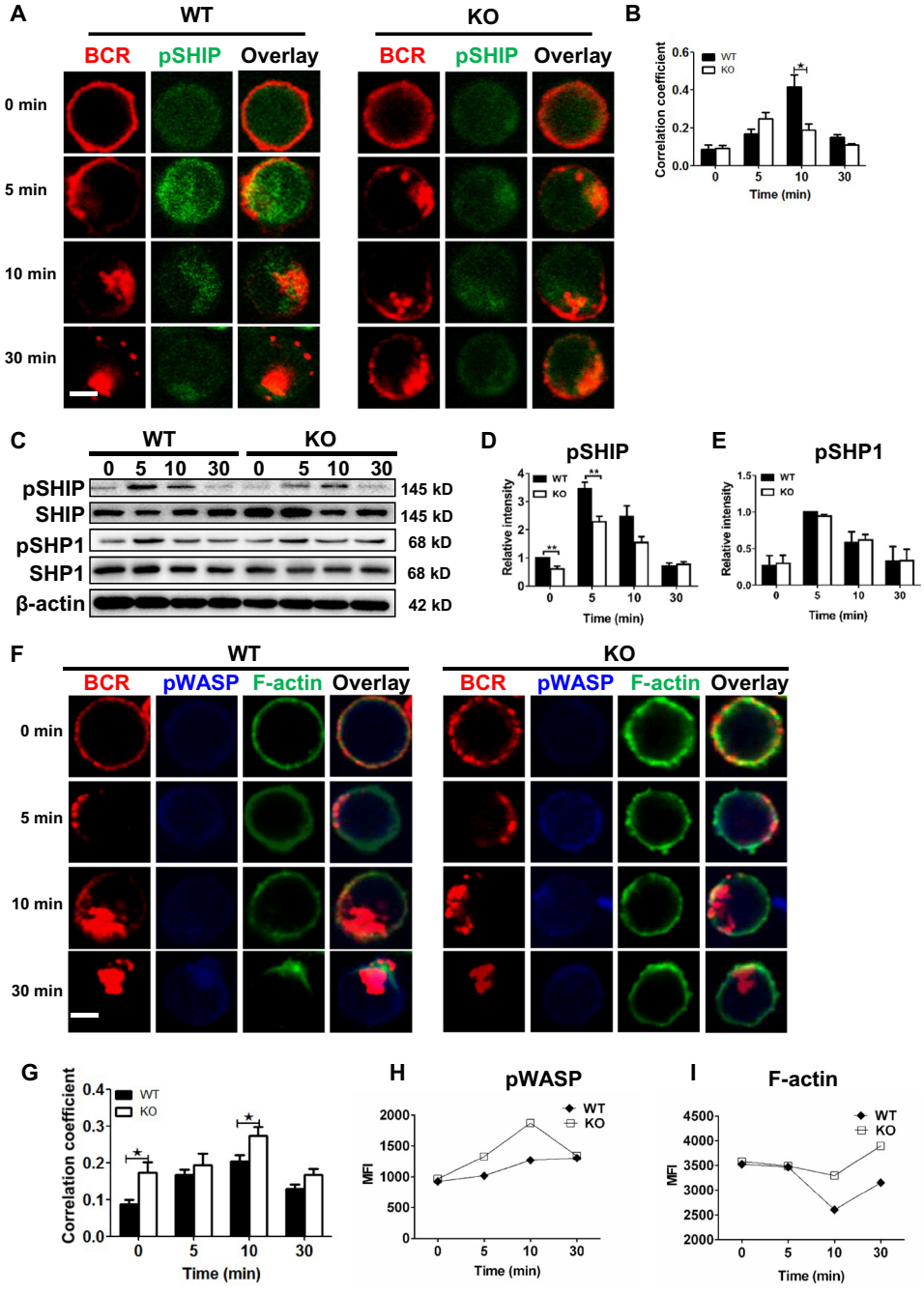

Fig. 4. STING deficiency down-regulates the activation of negative BCR signaling molecule, SHIP, and up-regulates the actin polymerization via enhancing the activation of WASP. Confocal analysis of splenic B cells from WT and KO mice labeled with AF546-mB-Fab-anti-Ig and then incubated without or with streptavidin for activation. Cells were fixed, permeabilized, and stained with Abs specific for pSHIP, pWASP, and F-actin (**A** and **F**). Splenic B cells from WT and *Sting* KO mice were activated with biotin-conjugated $F(ab')_2$ anti-mouse Ig(M + G) plus streptavidin for indicated times. Cell lysates were analyzed using SDS-PAGE and Western blot and probed for pSHIP/SHIP, pSHP1/SHP1 (**C**). Total protein or β-actin was used as controls. Shown are representative images, blots, and the correlation coefficients between the labeled BCR and pSHIP (**B**), pWASP (**G**), as well as the relative intensity of bands from immunoblots (**D** and **E**) taken from three independent experiments. Splenic B cells were labeled with anti-B220 and stimulated with sAg for indicated times and then stained with phalloidin and antibody specific for pWASP for phos flow cytometry. MFI of pWASP and F-actin in B cells was quantified using FlowJo software (**H** and **I**). Shown are levels of pWASP and F-actin from one of three independent experiments. Scale bars, 2.5 μm. $^*P < 0.05$; $^{**}P < 0.01$.

that the colocalization of PI3K or pPI3K with the BCR was not altered in *Sting* KO B cells for any of the time points examined (fig. S6, A to D). Next, we determined the PI3K activity by measuring PI(3,4)P2 levels using flow cytometry. The levels of PI(3,4)P2 were reduced in *Sting* KO B cells upon antigenic stimulation at 5 min (fig. S6E). These results suggest that STING directly affects the activity of PI3K. Next, we determined which signaling molecule recruits STING to the BCR by using specific inhibitors for Syk, PI3K,

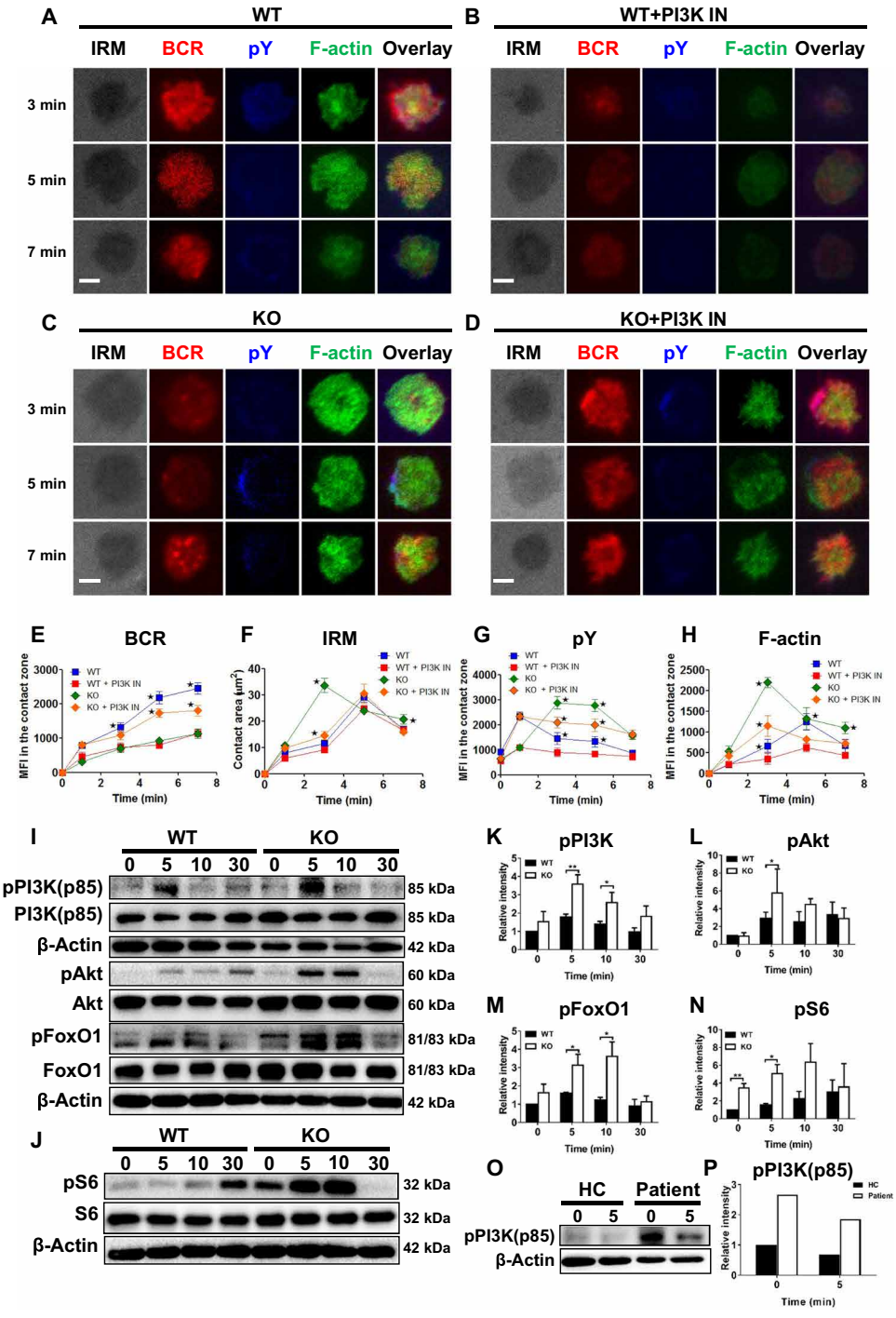

Fig. 5. PI3K inhibition rescues the abnormal accumulation of F-actin in *Sting* KO B cells. Splenic B cells from WT and *Sting* KO mice, pretreated with or without PI3K inhibitor, were incubated with AF546-mB-Fab-anti-Ig tethered to lipid bilayers with varying lengths of time and then fixed, permeabilized, and stained with antibodies specific for pY and F-actin. Cells were analyzed using TIRFm. Shown are representative images (**A** to **D**), the average values of the B cell contact area (**F**), and the MFI of the pY (**G**), BCR (**E**), and F-actin (**H**) in the contact zone. Scale bars, 2.5 μm. Splenic B cells from WT and *Sting* KO mice were activated with biotin-conjugated F(ab')$_2$ anti-mouse Ig(M + G) plus streptavidin for indicated times. Cell lysates were analyzed using SDS-PAGE and Western blot and probed for pPI3K (p85)/PI3K (p85), pAtk/Akt, pS6/S6 (**I**), and pFoxO-1/FoxO-1 (**J**). Total protein or β-actin was used as controls. Shown are representative blots from three independent experiments and blots' relative intensity (**K** to **N**). Western blot analysis the level of pPI3K in purified B cells from PBMCs of the healthy control and *STING* mutant patient (**O** and **P**). $^{*}P < 0.05$; $^{**}P < 0.01$.

and Lyn. WT B cells were treated with inhibitors and examined for colocalization between the BCR and STING. We found that the treatment with PI3K inhibitors largely reduced the colocalization between the BCR and STING compared with the treatment of Lyn and Syk inhibitors (fig. S6, F to J). Together, these results suggest that PI3K is largely responsible for recruiting STING to the BCR. Together, these results suggest that STING uses PI3K as the central hub for regulating the actin reorganization that offers feedback to the BCR clustering and BCR signaling.

STING deficiency causes a reduced humoral immune response

To further investigate the effect of STING deficiency on the humoral immune response, we immunized mice with 4-Hydroxy-3-nitrophenylacetyl-Keyhole Limpet Hemocyanin (NP-KLH) to analyze the T cell–dependent immune response. After 14 days of immunization, the mice were euthanized and splenocytes and serum were harvested for flow cytometry and serological analysis. After immunization, the frequency of FO B cells was decreased in both WT and KO mice, but the absolute number of FO B cells was decreased in KO mice compared with that of WT mice (Fig. 6, A and B). The number and percentage of MZ B cells were both decreased in KO mice compared with WT mice after immunization. In addition, the number and percentage of MZ B cells were decreased in immunized KO mice compared with nonimmunized (Fig. 6, C and D). The frequency and number of T1 cells were increased only in immunized WT mice, and the frequency and number of T2 cells were increased both in WT and KO mice after immunization. Furthermore, the frequency of T2 cells was increased in immunized KO mice compared with WT mice (Fig. 6, E and F). The frequency and number of GC B cells were decreased in KO mice compared to WT mice after immunization, but the percentage and number of GC B cells were only increased in WT mice after immunization in contrast to nonimmunized mice (Fig. 6, G and H). To further characterize the GC kinetics in *Sting* KO mice, we immunized the mice at days 5, 10, and 15 and then collected the splenocytes and serum for flow cytometry and ELISA. We found that the increase in the percentage of GC B cells in *Sting* KO mice was less than that in WT mice, although the percentage of GC B cells was higher in *Sting* KO mice at time zero (fig. S7A). The titers of NP-IgG antibody were significantly lower at days 5, 10, and 15 in *Sting* KO mice compared with WT mice (fig. S7B). In addition, the percentage and number in MBCs and plasma cells (PCs) after immunization had no changes compared with WT mice (Fig. 6, I to L). We further characterized the MBCs with CD80 and PD-L2, and still, no difference was observed between WT and KO mice (fig. S7, C and D). However, no difference in the frequency and number was observed for switched and unswitched between WT and KO mice after immunization (fig. S7, E to G). Last, we found that the titers of NP-specific IgG1 and IgM were both decreased in KO mice compared with that of WT mice after 14 days of immunization (Fig. 6, M and N), which is consistent with the immunization results from DNA vaccine encoding ovalbumin (*29*). Because *Sting* KO is systemic, several of the phenotypes observed including GC B cell population expansion and the responses to NP-KLH would require the involvement of T cells. Thus, we examined the percentage and number of follicular helper T (Tfh) cells, and no difference was observed between WT and *Sting* KO mice after NP-KLH immunization (fig. S7, H and I). These results indicate that the phenotype in *Sting* KO mice is probably due to a B cell–intrinsic activation defect. These results suggest that STING is required for an efficient humoral immune response elicited by T cell–dependent antigens.

DISCUSSION

In our study, we investigated the effect of the loss of STING on BCR signaling and the underlying molecular mechanisms. We found that STING negatively regulates BCR signaling by suppressing the CD19-PI3K-Btk proximal axis and the Akt-mTORC1 distal axis, and by enhancing the activation of SHIP, which also negatively regulates the actin reorganization. The inhibition of PI3K rescues the abnormal actin reorganization, which offers feedback to obtain the recovered BCR signaling and early B cell activation. Therefore, our study has provided a new regulatory mechanism of STING on BCR signaling as well as actin reorganization.

We have shown that STING can regulate the activation of WASP and resultant actin reorganization. It is the first time that STING was linked to the actin cytoskeleton. Previous research demonstrated that STING is correlated with the activation of autophagy that needs remodeling of the actin cytoskeleton (*30*). STING colocalizes with microtubule-associated protein 1 light chain 3 (LC3) and autophagy-related gene 9a (Atg9a) after sensing dsDNA (*30*). But the underlying molecular mechanism is unknown. It would be interesting to examine whether STING is involved in the BCR endocytosis that is critical to form the endosomal/lysosomal vesicles for autophagy. Our previous research has shown that the reduced BCR endocytosis up-regulates the BCR signaling (*31*–*33*). This may also contribute to the enhanced BCR signaling in *Sting* KO B cells. Another experiment to do is to inhibit the overactivated WASP and enhanced actin accumulation in STING with in vivo treatments of latrunculin B (*19*). Additional experiments to perform may include possibly rescuing the *Sting* KO phenotype by crossing the *Sting* KO mice with *Wasp* KO mice and then examining the early activation of these B cells, including BCR clustering and B cell spreading, as well as the differentiation of MZ B cells and lupus development. On the basis of what has been observed, it might be insightful to investigate whether STING regulates other actin regulators, such as ezrin or Abp1.

The *Sting* KO mice have a germline deletion; therefore, there is a possibility that other lymphocytes also have a similar phenotype to that observed in the KO mice. It has been reported that the strength of STING activation determines $CD8^+$ T cell–mediated antitumor immunity (*34*). We examined most of the T cell populations and did not find any changes in the amount of CD4, CD8, and T_{regs} in KO mice. The antibody response to T-dependent antigen was reduced in *Sting* KO mice. This result may be due to a number of factors including *Sting* KO in T cells, as well as ongoing autoimmunity and the narrowing of the B cell repertoire. Furthermore, we examined the Tfh cells that are crucial for the T cell–dependent antigen response of B cells. Still, no difference was observed between WT and *Sting* KO mice, so it is possible that the majority of the B cell phenotype observed in *Sting* KO mice is B cell intrinsic.

Another remaining issue is how STING regulates the phosphorylation of CD19. STING mediates the type I interferon immune response by acting as a direct DNA sensor and a signaling adaptor protein. STING stimulates TBK1 activity to phosphorylate IRF3 or STAT6 (signal transducer and activator of transcription 6) upon stimulation with dsDNA. Phosphorylated IRF3s and STAT6s undergo dimerization and then enter the nucleus to trigger the expression of genes such

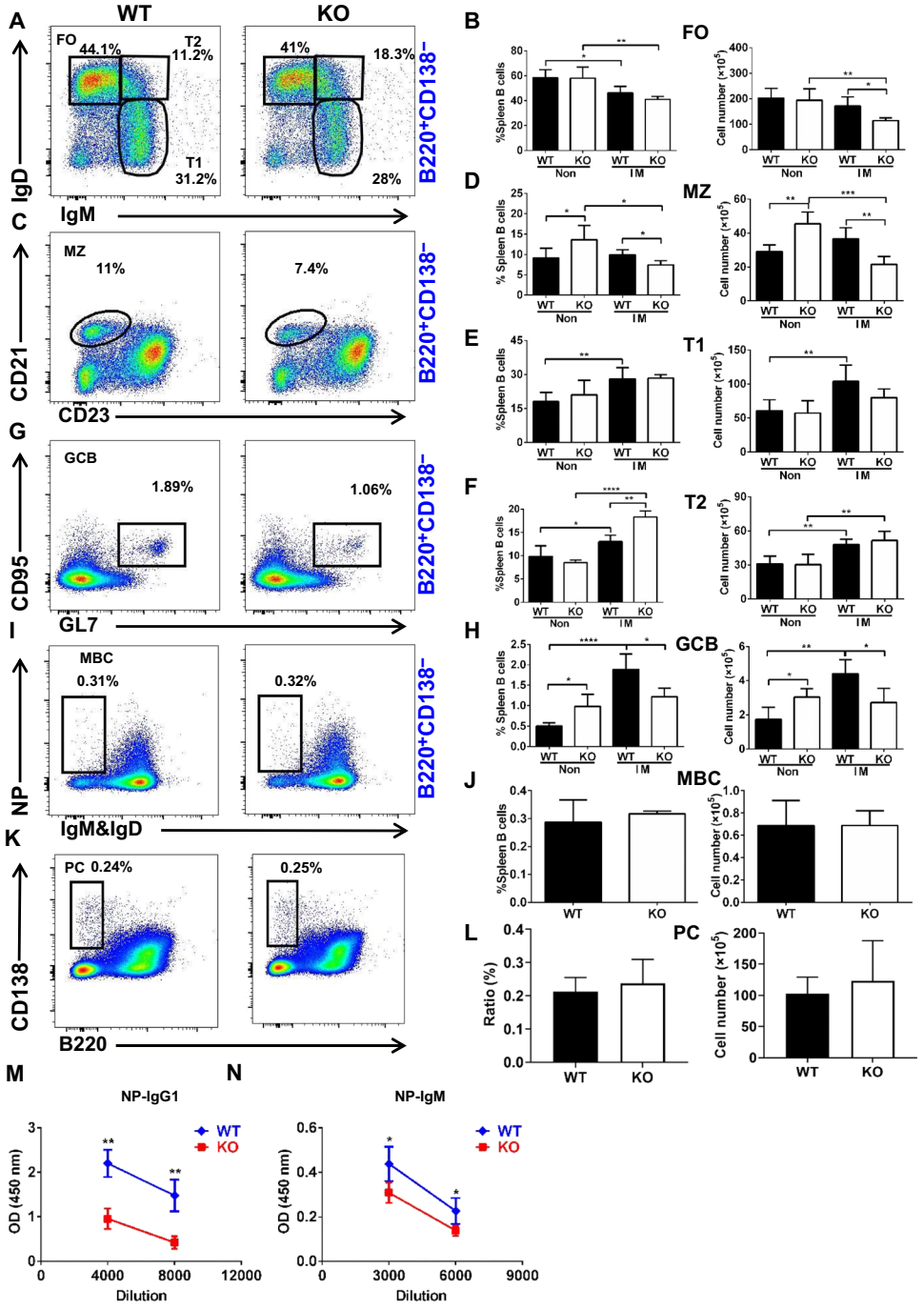

Fig. 6. STING deficiency reduces the T-dependent Ab responses. Flow cytometry analysis of splenic cells from immunized WT and *Sting* KO mice ($n = 4$) for FO B, MZ B, T1 B, T2 B, GC B, MBCs, and PCs. Shown are representative dot plots, the average percentages (±SD) and numbers of subpopulations (**A** to **L**). ELISA analysis ($n = 4$) of NP-specific IgG1 and NP-specific IgM in the serum (**M** and **N**). *$P < 0.05$; **$P < 0.01$; ***$P < 0.001$; ****$P < 0.0001$.

as IFNB, CCL2, and CCL20 (*35*, *36*). STING may also inhibit the upstream kinase activity of CD19, which is why the deficiency of STING causes enhanced phosphorylation of CD19. Another key point is that STING-mediated PI3K signaling is required to regulate the activation of WASP and the resultant actin reorganization. It would be interesting to treat mice with PI3K inhibitor in vivo, or by crossing the *Sting* KO mice with PI3K mutant mice such as p110δ-deficient mice, and examine the early activation of B cells and actin reorganization as well as the B cell differentiation and autoimmune phenotype in mice.

Another interesting finding in this study is that the enhanced BCR signaling in *Sting* KO mice caused reduced GC formation and antigen-specific antibody production. These results indicate that generation of GCs and antigen-specific antibodies needs a specific window of BCR signaling. Too strong or too low of BCR signaling leads to the impaired generation of GCs and PCs, which causes lower

production of antigen-specific antibodies. All these results fit the findings from Westerberg and co-workers (*37*, *38*). In the *STING* mutant patient, we also found a reduction in unswitched and MBCs in the physiological situation, which may explain the decreased antibody production in the *Sting* KO mice.

Overall, our study linked the key adaptor protein, STING, to its role in B cell adaptive immunity. We found that it can modulate the BCR signaling via PI3K that regulates the actin reorganization via WASP. The regulation of STING on BCR signaling leads to the control of humoral immune response. All of these findings will provide insight for additional STING studies in the innate immunity field.

METHODS

Mice and patients

Sting KO mice on the C57BL/6 background were donated by H. Shu's laboratory in Wuhan University of China (*39*). BAC (bacterial artificial chromosome)–retrieval methods were used for constructing the targeting vector. In brief, the *Sting* gene was retrieved from a C57BL/6J BAC clone RP24-368N11 (provided by BACPAC Resource Center) by a retrieval vector containing two homologous arms. After correct recombination, the vector contained 15.5 kb of genomic sequence including 5.2-kb upstream sequences, exons II to VI, and 5.8-kb downstream sequences. The entire exon II–VI was then deleted and replaced with a loxP-Neo-loxP cassette. The targeting construct, which contains a neomycin expression cassette for positive selection and an HSV-tk expression cassette for negative selection, was linearized with Not I restriction enzyme and electroporated into C57BL/6-derived B6/BLU embryonic stem (ES) cells. Seventy-six ES cell clones were selected and verified for correct recombination with long-range polymerase chain reaction (PCR) and Southern blot analysis. Correctly targeted ES cells were injected into C57BL/6J blastocysts followed by transfer to pseudopregnant mice. Chimeric male mice identified by PCR were bred to C57BL/6J females to generate F1 offspring. Germline transmission of the targeted *Sting* allele was verified by PCR analysis of tail DNA from F1 offspring. The heterozygous mice were interbred to obtain WT, heterozygous and homozygous littermates (KO). All mice were fed and maintained under the specific pathogen–free condition. All mouse experiments were performed according to the guidelines of the Chinese Council on Animal Care and approved by the Ethics Committee of Animal Experimentation of Tongji Medical College (Wuhan, China).

An 8-month-old Chinese patient with *STING* mutations (*Tmem173* c.461A>G, p.Asn154Ser) and an age-matched healthy control subject were involved in this study. All subjects provided written informed consent by their parents with the approval of the Ethics Committee of the Huazhong University of Science and Technology.

Purification of B cells

Splenic lymphocytes were isolated by Ficoll density centrifugation according to standard protocols. Splenic B cells were purified through deleting T cells by anti-Thy1.2 monoclonal antibody (mAb) (BioLegend) and guinea pig complement (Rockland Immunochemicals) and then incubated at 37°C for 1 hour. PBMCs from patient and HC were isolated by sucrose density gradient centrifugation, and enriched B cells were sorted by CD19 MicroBeads for human kit (130-050-301, Miltenyi) according to standard protocols.

Preparation of monobiotinylated Fab' Ab and Ag-tethered planar lipid bilayers

The planar lipid bilayer and liposomes were prepared as described previously (*20*). The $F(ab')_2$ fragment (Jackson ImmunoResearch Laboratories) was used for making the monobiotinylated Fab' fragment of anti-mouse IgM + G Ab (mB-Fab'-anti-Ig) following a published protocol (*40*). To break the disulfide bond that links the two Fab', 20 mM 2-mercaptoethylamine was used, and the reduced cysteine was biotinylated by maleimide-activated biotin (Thermo Fisher Scientific). Next, Fab' was purified, quantified, and labeled with Alexa Fluor 546 (Thermo Fisher Scientific). To activate B cells with sAg, splenic B cells were labeled with AF546-mB-Fab'-anti-Ig (2 μg/ml) and added in mB-Fab'-anti-Ig (8 μg/ml) for 30 min and streptavidin (1 μg/ml) for 10 min at 4°C. As a control, streptavidin was omitted. Cells were incubated at 37°C for indicated times. To activate B cells with mAg, cells were incubated with AF546-mB-Fab'-anti-Ig and mB-Fab'-anti-Ig tethered to planar lipid bilayers by streptavidin at 37°C for varying lengths of time.

Confocal and TIRF microscopy

For confocal analysis, purified splenic B cells were stained with anti-CD16/CD32 mAb (BioLegend) to block Fcγ receptors and stimulated with AF546-mB-Fab'-anti-Ig with or without streptavidin (sAg) at 4°C. Cells were chased for 0, 5, 10, and 30 min at 37°C. After stimulation, cells were fixed with 4% paraformaldehyde (Thermo Fisher Scientific), permeabilized with 0.05% saponin (S4521-10G, Sigma-Aldrich), and stained for anti-STING (NBP2-24683SS, Novus Bio), ER-Tracker dyes (E12353, Invitrogen), anti-phosphotyrosine (pY, 05-321, Merck Millipore), anti-pBtk (ab52192, Abcam), anti-pCD19 (ab63443, Abcam), anti-pSHIP1 (3941s, Cell Signaling Technology), anti-PI3K (4292 s, Cell Signaling Technology), anti-pPI3K (4228s, Cell Signaling Technology), AF488-phalloidin (R37110, Thermo Fisher Scientific), and anti-pWASP (A300-205A, Bethyl) and analyzed using a confocal microscope (Zeiss, LSM 780) with 405-, 488-, and 546-nm lasers. Colocalization was determined using the ZEN 2.3 (blue edition) software.

For TIRFm analysis, to image intracellular protein, B cells with or without PI3K inhibitor treatment were activated with an Ag-tethered lipid bilayer at 37°C for indicated times. Cells were then fixed, permeabilized, and stained for pY and AF488-phalloidin. Images were acquired using the TIRFm (Nikon Eclipse Ti-PFS). The B cell contact area was determined and analyzed using interference reflection microscopy images and NIS-Elements AR 3.2 software. MFI of each image in the B cell contact zone was determined using the same software. Background generated by Ag tethered to lipid bilayers in the absence of B cells controls was subtracted. For each set of data, more than 50 individual cells from three independent experiments were analyzed.

Flow cytometry and phos flow

The red blood cells in collected BM cells from two mouse legs were lysed with ACK Lysis Buffer (RT122-02, TIANGEN). For B cell subset analysis, BM cells and splenic cells were incubated with anti-mouse CD16/CD32. BM cells were stained with antibodies including allophycocyanin (APC)–anti-CD43, PB-anti-IgM, PE-anti-BP1, PerCP-anti-B220, PE/Cy7-anti-CD24, and fluorescein isothiocyanate (FITC)–anti-CD127 (BioLegend). Splenic lymphocytes were stained with the following antibodies: FITC-anti-CD19, FITC-anti-CD95, FITC–anti–annexin V, FITC-anti-B220, Percp-anti-B220, BV510-anti-B220, PE-anti-CD23, Percp-anti-IgD, APC-anti-CD21, AF647-anti-GL7, PB-anti-IgM, PE-Cy7-PD-L2 APC-CD73, and

BV510-CD80 (104741, BioLegend). For intracellular staining (PE-Cy7-anti-ki67, eBioscience), cells were fixed and permeabilized with a Fixation/Permeabilization Kit (00-5123, 00-5223, eBioscience) and washed with permeabilization buffer (00-8333, eBioscience). To analyze splenic MBC, PBC, and PC B cells, anti-mouse Abs were used, including PE-NP (Biosearch Technologies), BV510-anti-CD138 (BioLegend), and PB-anti-IgD (BioLegend).

For Phosflow, primary B cells were incubated with biotin-conjugated $F(ab')_2$ anti-mouse Ig(M + G) (115-066-068, Jackson ImmunoResearch) plus streptavidin at 37°C for varying lengths of time. Cells were fixed with Phosflow Lyse/Fix buffer, permeabilized with Phosflow Perm buffer III (BD Biosciences), and labeled with AF488-phalloidin, anti-pWASP, and PE-PIP2 (Ab01220-10.0, Absolute Antibody).

For T cell subsets analysis, isolated lymphocytes from thymus, spleen, and LNs were stained with PE-anti-CD4 (BioLegend, 100408), Pacific Blue-anti-CD4 (BioLegend, 100531), Brilliant Violet 510-anti-CD8a (BioLegend, 100751), APC/Cy7-anti-TCRβ (BioLegend, 109220), 7-AAD (BD Pharmingen, 559925), APC-anti-CD25 (BioLegend, 102012), PerCP/Cy5.5-anti-CD44 (BioLegend, 103032), PE/Cy7-anti-CD62L (BioLegend, 104418), PE-anti-CD278 (ICOS) (BioLegend, 107705), APC-anti-CD304 (Neuropilin-1, Nrp1) (BioLegend, 145206), and PE/Cy7-anti-CD279 (PD-1) (BioLegend, 109110). For intracellular staining, cells were fixed and permeabilized with Fixation/Permeabilization Kit (eBioscience, 00-5123, 00-5223), washed with permeabilization buffer (eBioscience, 00-8333), and stained with PE-anti-CTLA4 (BioLegend, 106306) and AF488-anti-Foxp3 (Thermo Fisher Scientific, 53-5773-82).

For T cell intracellular cytokine analysis, lymphocytes from thymus, spleen, and LNs were stimulated with PMA (phorbol 12-myristate 13-acetate) (50 ng/ml; Sigma-Aldrich, P1585-1MG), GolgiStop (1:1000; BD Biosciences, 554724), and ionomycin (1 μM; CST, 9995S) for 5 hours at 37°C, 5% CO_2, and then cells were collected and stained with PE-anti-CD4 (BioLegend, 100408), Brilliant Violet 510-anti-CD8a, PerCP/Cy5.5-anti-CD44, and APC/Cy7-anti-TCRβ. After this, cells were fixed, permeabilized, and stained with APC-anti-IL-4 (BioLegend, 504106), PE/CY7-anti-IFN-γ (BioLegend, 505826), and Brilliant Violet 421-anti-IL-17A (BioLegend, 506925).

For Tfh cell analysis, splenic lymphocytes were prestained with CXCR5 (551961, BD Biosciences) at 4°C for 1 hour and then stained for Biotin-SP AffiniPure $F(ab')_2$ Fragment goat anti-rat IgG (H + L) (112-066-003, Jackson ImmunoResearch) at 4°C for 30 min, followed by DyLight 405 SA (016-470-084,), APC-anti-CD4 (100411, BioLegend), Percp-anti-CD44, PE-Cy7-anti-PD-1, and PE-ICOS. Cells were analyzed by an LSR II multicolor flow cytometer (BD Biosciences, CA, USA), and data analysis was performed using the FlowJo software (TreeStar, USA) as previously described (*19*).

Generation of BM chimeras

BM cells from femurs of 8-week-old CD45.2 WT, CD45.1 WT, and CD45.2 *Sting* KO mice were collected, and then CD45.2 WT or CD45.2 *Sting* KO BM cells were mixed with CD45.1 WT BM cells at a 1:1 ratio. Mixed BM cells (5×10^6) were intravenously injected into 8-week-old CD45.1 WT recipients that were sublethally irradiated (7 Gy). Eight weeks after BM reconstitution, splenic cells from recipients were isolated for further analysis.

Western blot analysis

Purified B cells were activated with biotin-conjugated $F(ab')_2$ anti-mouse Ig(M + G) or biotin-conjugated $F(ab')_2$ anti-human Ig(M + G) plus streptavidin for indicated times. The cell lysates were separated by SDS–polyacrylamide gel electrophoresis, transferred onto a nitrocellulose membrane, and probed with anti-pY (05-321, Merck Millipore), anti-pBtk (ab52192, Abcam), anti-Btk (8547S, Cell Signaling Technology), anti-pCD19 (3571S, Cell Signaling Technology), anti-pSHIP1 (3941S, Cell Signaling Technology), anti-SHIP1 (2728S, Cell Signaling Technology), anti-pPI3K p85/p55 (4228S, Cell Signaling Technology), anti-PI3K p85 (4292S, Cell Signaling Technology), anti-pAkt (4060L, Cell Signaling Technology), anti-Akt (9272S, Cell Signaling Technology), anti-pS6 (4856S, Cell Signaling Technology), anti-S6 (2217S, Cell Signaling Technology), anti-pFoxO1 (9461S, Cell Signaling Technology), anti-FoxO1 (2880S, Cell Signaling Technology), anti-pSyk (2710S, Cell Signaling Technology), anti-Syk (13198S, Cell Signaling Technology), anti-pSHP1 (8849S, Cell Signaling Technology), and SHP1 (14074S, Cell Signaling Technology). In addition, WT and KO splenic cell lysates were incubated with anti-STING. β-Actin was used as the loading control for the amount of total protein. Immunoreactive bands were captured with the ChemiDoc XRS+ imaging systems (Bio-Rad). The levels were quantified by densitometry using Image Lab software (Bio-Rad), normalized against β-actin or total protein, and expressed as fold increases over 0 min of WT.

Immunization and ELISA

For NP-KLH immunization, a mixture of NP-KLH/adjuvant (MPL + TDM, S6322, Sigma-Aldrich) was prepared according to the specification with a concentration of NP-KLH (0.2 mg/ml; N-5060-25, Biosearch). WT and *Sting* KO mice aged 6 to 8 weeks were injected subcutaneously with 200 μl of the mixture. Two weeks later, the spleen was harvested and splenic lymphocytes were collected with Ficoll for flow cytometry analysis. To measure the antibody levels of NP-specific subclasses, the diluted serum was analyzed by ELISA using NP–bovine serum albumin (BSA) (2 g/ml; Biosearch Technologies)–coated plates and IgM- and IgG1-specific secondary Ab (1:5000; Bethyl Laboratories).

Anti-dsDNA analysis

To evaluate the serum levels of anti-dsDNA antibody, 96-well plates (Nunc MaxiSorp Immuno) were precoated with calf thymus dsDNA (100 g/ml; Academy Bio-Medical) at 4°C overnight and blocked with 0.5% BSA/phosphate-buffered saline. Diluted serum (1:200) of WT and KO mice was added and then plates were incubated with goat anti-mouse IgG–horseradish peroxidase (HRP) (1:2000; 1030-05, Southern Biotechnology). After reaction with TMB substrate (555214, BD Bioscience), OD450 was measured using microplate reader (PerkinElmer) following the protocol as descripted (*31*).

Immunofluorescence analysis of spleen and kidney

Spleens and kidneys of WT and *Sting* KO mice were embedded in OCT, frozen in liquid nitrogen, and stored at −80°C. Next, samples were cut into 5-μm sections on a cryostat and fixed with acetone for 5 min, dried at room temperature, and stored at −80°C for immunofluorescence staining. After blocking with 5% BSA, sections from spleens and kidneys were stained respectively with AF488-GL7 (1:20; 562080, BD Bioscience), PE-CD4 (1:20; 12-0042-83, eBioscience) as well as biotin-IgD (1:50; 13-5993-85, eBioscience), Alexa Fluor 488–AffiniPure donkey anti-mouse IgG (H + L) (1:200; 715-545-151, Jackson), or complement C3 (1:400; NB200-540, Novus) for 30 min at room temperature and then incubated with Dy510-avidin (1:500; 84547, Pierce) or AF488 goat anti-rat IgG (H + L) (1:400; A11006,

Thermo Fisher Scientific). All slides were washed and covered with imaging antifade reagent to prevent fluorescence quenching. Images were captured using a confocal microscope (Zeiss, LSM 780) and analyzed with the ZEN 2.3 (blue edition) software.

Treatment with PI3K, Lyn, and Syk inhibitors in vitro

B cells were pretreated with 3 μM of the p110δ specific inhibitor IC87114 (528118, Calbiochem), 1 μM of the Lyn inhibitor (T6311, TargetMol), or 5 μM of the Syk inhibitor (T6101, TargetMol) for 30 min before and during the stimulation.

Statistical analysis

Unpaired two-tailed Student's *t* test was carried out for comparisons between two groups. Analysis of variance (ANOVA) test was used for comparisons between more than two groups. Statistical significance was assessed with GraphPad Prism 6 Software (San Diego, CA). Experimental values are presented as means ± SD. The difference was considered significant when $P < 0.05$. $^{*}P < 0.05$, $^{**}P < 0.01$, $^{***}P < 0.001$, $^{****}P < 0.0001$.

SUPPLEMENTARY MATERIALS

Supplementary material for this article is available at http://advances.sciencemag.org/cgi/content/full/6/17/eaax9455/DC1

View/request a protocol for this paper from *Bio-protocol*.

REFERENCES AND NOTES

1. H. Ishikawa, G. N. Barber, Erratum: STING is an endoplasmic reticulum adaptor that facilitates innate immune signalling. *Nature* **455**, 674–678 (2008).
2. G. N. Barber, Innate immune DNA sensing pathways: STING, AIMII and the regulation of interferon production and inflammatory responses. *Curr. Opin. Immunol.* **23**, 10–20 (2011).
3. B. Zhong, Y. Yang, S. Li, Y.-Y. Wang, Y. Li, F. Diao, C. Lei, X. He, L. Zhang, P. Tien, H.-B. Shu, The Adaptor Protein MITA Links Virus-Sensing Receptors to IRF3 Transcription Factor Activation. *Immunity* **29**, 538–550 (2008).
4. A. Gall, P. Treuting, K. B. Elkon, Y.-M. Loo, M. Gale Jr., G. N. Barber, D. B. Stetson, Autoimmunity initiates in nonhematopoietic cells and progresses via lymphocytes in an interferon-dependent autoimmune disease. *Immunity* **36**, 120–131 (2012).
5. Y. Liu, A. A. Jesus, B. Marrero, D. Yang, S. E. Ramsey, G. A. Montealegre Sanchez, K. Tenbrock, H. Wittkowski, O. Y. Jones, H. S. Kuehn, C.-C. R. Lee, M. A. DiMattia, E. W. Cowen, B. Gonzalez, I. Palmer, J. J. DiGiovanna, A. Biancotto, H. Kim, W. L. Tsai, A. M. Trier, Y. Huang, D. L. Stone, S. Hill, H. J. Kim, C. St. Hilaire, S. Gurprasad, N. Plass, D. Chapelle, I. Horkayne-Szakaly, D. Foell, A. Barysenka, F. Candotti, S. M. Holland, J. D. Hughes, H. Mehmet, A. C. Issekutz, M. Raffeld, J. McElwee, J. R. Fontana, C. P. Minniti, S. Moir, D. L. Kastner, M. Gadina, A. C. Steven, P. T. Wingfield, S. R. Brooks, S. D. Rosenzweig, T. A. Fleisher, Z. Deng, M. Boehm, A. S. Paller, R. Goldbach-Mansky, Activated STING in a vascular and pulmonary syndrome. *N. Engl. J. Med.* **371**, 507–518 (2014).
6. N. Jeremiah, B. Neven, M. Gentili, I. Callebaut, S. Maschalidi, M.-C. Stolzenberg, N. Goudin, M.-L. Frémond, P. Nitschke, T. J. Molina, S. Blanche, C. Picard, G. I. Rice, Y. J. Crow, N. Manel, A. Fischer, B. Bader-Meunier, F. Rieux-Laucat, Inherited STING-activating mutation underlies a familial inflammatory syndrome with lupus-like manifestations. *J. Clin. Invest.* **124**, 5516–5520 (2014).
7. J. Ahn, P. Ruiz, G. N. Barber, Intrinsic self-DNA triggers inflammatory disease dependent on STING. *J. Immunol.* **193**, 4634–4642 (2014).
8. G. Dong, M. You, L. Ding, H. Fan, F. Liu, D. Ren, Y. Hou, STING Negatively Regulates Double-Stranded DNA-Activated JAK1-STAT1 Signaling via SHP-1/2 in B Cells. *Mol. Cells* **38**, 441–451 (2015).
9. C. L. Carpenter, B. C. Duckworth, K. R. Auger, B. Cohen, B. S. Schaffhausen, L. C. Cantley, Purification and characterization of phosphoinositide 3-kinase from rat liver. *J. Biol. Chem.* **265**, 19704–19711 (1990).
10. E. Clayton, G. Bardi, S. E. Bell, D. Chantry, C. P. Downes, A. Gray, L. A. Humphries, D. Rawlings, H. Reynolds, E. Vigorito, M. Turner, A crucial role for the p110δ subunit of phosphatidylinositol 3-kinase in B cell development and activation. *J. Exp. Med.* **196**, 753–763 (2002).
11. D. A. Tuveson, R. H. Carter, S. P. Soltoff, D. T. Fearon, CD19 of B cells as a surrogate kinase insert region to bind phosphatidylinositol 3-kinase. *Science* **260**, 986–989 (1993).
12. A. N. Anzelon, H. Wu, R. C. Rickert, P*ten* inactivation alters peripheral B lymphocyte fate and reconstitutes CD19 function. *Nat. Immunol.* **4**, 287–294 (2003).
13. B. Hebeis, E. Vigorito, D. Kovesdi, M. Turner, Vav proteins are required for B-lymphocyte responses to LPS. *Blood* **106**, 635–640 (2005).
14. D. C. Otero, S. A. Omori, R. C. Rickert, Cd19-dependent activation of Akt kinase in B-lymphocytes. *J. Biol. Chem.* **276**, 1474–1478 (2001).
15. A. Brunet, A. Bonni, M. J. Zigmond, M. Z. Lin, P. Juo, L. S. Hu, M. J. Anderson, K. C. Arden, J. Blenis, M. E. Greenberg, Akt promotes cell survival by phosphorylating and inhibiting a Forkhead transcription factor. *Cell* **96**, 857–868 (1999).
16. V. L. J. Tybulewicz, Commentary: New insights into the complexity of phosphatidylinositol lipid signaling in B lymphocytes. *Eur. J. Immunol.* **34**, 2964–2967 (2004).
17. K. E. O'Reilly, F. Rojo, Q.-B. She, D. Solit, G. B. Mills, D. Smith, H. Lane, F. Hofmann, D. J. Hicklin, D. L. Ludwig, J. Baselga, N. Rosen, mTOR inhibition induces upstream receptor tyrosine kinase signaling and activates Akt. *Cancer Res.* **66**, 1500–1508 (2006).
18. J. Jozwiak, S. Jozwiak, T. Grzela, M. Lazarczyk, Positive and negative regulation of TSC2 activity and its effects on downstream effectors of the mTOR pathway. *Neuromolecular Med.* **7**, 287–296 (2005).
19. L. Huang, Y. Zhang, C. Xu, X. Gu, L. Niu, J. Wang, X. Sun, X. Bai, X. Xuan, Q. Li, C. Shi, B. Yu, H. Miller, G. Yang, L. S. Westerberg, W. Liu, W. Song, X. Zhao, C. Liu, Rictor positively regulates B cell receptor signaling by modulating actin reorganization via ezrin. 15, e2001750 (2017).
20. C. Liu, X. Bai, J. Wu, S. Sharma, A. Upadhyaya, C. I. M. Dahlberg, L. S. Westerberg, S. B. Snapper, X. Zhao, W. Song, N-wasp is essential for the negative regulation of B cell receptor signaling. *PLOS Biol.* **11**, e1001704 (2013).
21. C. Liu, H. Miller, K. L. Hui, B. Grooman, S. Bolland, A. Upadhyaya, W. Song, A balance of Bruton's tyrosine kinase and SHIP activation regulates B cell receptor cluster formation by controlling actin remodeling. *J. Immunol.* **187**, 230–239 (2011).
22. S. Sharma, G. Orlowski, W. Song, Btk regulates B cell receptor-mediated antigen processing and presentation by controlling actin cytoskeleton dynamics in B cells. *J. Immunol.* **182**, 329–339 (2009).
23. M. D. Thomas, B. Srivastava, D. Allman, Regulation of peripheral B cell maturation. *Cell. Immunol.* **239**, 92–102 (2006).
24. S. Pillai, A. Cariappa, The follicular versus marginal zone B lymphocyte cell fate decision. *Nat. Rev. Immunol.* **9**, 767–777 (2009).
25. A. Cariappa, M. Tang, C. Parng, E. Nebelitskiy, M. Carroll, K. Georgopoulos, S. Pillai, The follicular versus marginal zone B lymphocyte cell fate decision is regulated by Aiolos, Btk, and CD21. *Immunity* **14**, 603–615 (2001).
26. N. Baumgarth, The double life of a B-1 cell: Self-reactivity selects for protective effector functions. *Nat. Rev. Immunol.* **11**, 34–46 (2011).
27. A. Cerutti, M. Cols, I. Puga, Marginal zone B cells: Virtues of innate-like antibody-producing lymphocytes. *Nat. Rev. Immunol.* **13**, 118–132 (2013).
28. D. O. Griffin, T. L. Rothstein, A small CD11b^{+}human B1 cell subpopulation stimulates T cells and is expanded in lupus. *J. Exp. Med.* **208**, 2591–2598 (2011).
29. H. Ishikawa, Z. Ma, G. N. Barber, STING regulates intracellular DNA-mediated, type I interferon-dependent innate immunity. *Nature* **461**, 788–792 (2009).
30. T. Saitoh, N. Fujita, T. Hayashi, K. Takahara, T. Satoh, H. Lee, K. Matsunaga, S. Kageyama, H. Omori, T. Noda, N. Yamamoto, T. Kawai, K. Ishii, O. Takeuchi, T. Yoshimori, S. Akira, Atg9a controls dsDNA-driven dynamic translocation of STING and the innate immune response. *Proc. Natl. Acad. Sci. U.S.A.* **106**, 20842–20846 (2009).
31. S. Becker-Herman, A. Meyer-Bahlburg, M. A. Schwartz, S. W. Jackson, K. L. Hudkins, C. Liu, B. D. Sather, S. Khim, D. Liggitt, W. Song, G. J. Silverman, C. E. Alpers, D. J. Rawlings, WASp-deficient B cells play a critical, cell-intrinsic role in triggering autoimmunity. *J. Exp. Med.* **208**, 2033–2042 (2011).
32. O. O. Onabajo, M. K. Seeley, A. Kale, B. Qualmann, M. Kessels, J. Han, T.-H. Tan, W. Song, Actin-binding protein 1 regulates B cell receptor-mediated antigen processing and presentation in response to B cell receptor activation. *J. Immunol.* **180**, 6685–6695 (2008).
33. M. K. Seeley-Fallen, L. J. Liu, M. R. Shapiro, O. O. Onabajo, S. Palaniyandi, X. Zhu, T.-H. Tan, A. Upadhyaya, W. Song, Actin-binding protein 1 links B-cell antigen receptors to negative signaling pathways. *Proc. Natl. Acad. Sci. U.S.A.* **111**, 9881–9886 (2014).
34. K. E. Sivick, A. L. Desbien, L. H. Glickman, G. L. Reiner, L. Corrales, N. H. Surh, T. E. Hudson, U. T. Vu, B. J. Francica, T. Banda, G. E. Katibah, D. B. Kanne, J. J. Leong, K. Metchette, J. R. Bruml, C. O. Ndubaku, J. M. McKenna, Y. Feng, L. Zheng, S. L. Bender, C. Y. Cho, M. L. Leong, A. van Elsas, T. W. Dubensky Jr., S. M. McWhirter, Magnitude of therapeutic STING activation determines CD8^{+} T cell-mediated anti-tumor immunity. *Cell Rep.* **29**, 785–789 (2019).
35. D. L. Burdette, R. E. Vance, STING and the innate immune response to nucleic acids in the cytosol. *Nat. Immunol.* **14**, 19–26 (2013).
36. H. Chen, H. Sun, F. You, W. Sun, X. Zhou, L. Chen, J. Yang, Y. Wang, H. Tang, Y. Guan, W. Xia, J. Gu, H. Ishikawa, D. Gutman, G. Barber, Z. Qin, Z. Jiang, Activation of STAT6 by STING is critical for antiviral innate immunity. *Cell* **147**, 436–446 (2011).

37. L. S. Westerberg, C. Dahlberg, M. Baptista, C. J. Moran, C. Detre, M. Keszei, M. A. Eston, F. W. Alt, C. Terhorst, L. D. Notarangelo, S. B. Snapper, Wiskott-Aldrich syndrome protein (WASP) and N-WASP are critical for peripheral B-cell development and function. *Blood* **119**, 3966–3974 (2012).
38. C. I. M. Dahlberg, M.-L. Torres, S. H. Petersen, M. A. P. Baptista, M. Keszei, S. Volpi, E. K. Grasset, M. C. I. Karlsson, J. E. Walter, S. B. Snapper, L. D. Notarangelo, L. S. Westerberg, Deletion of WASp and N-WASp in B cells cripples the germinal center response and results in production of IgM autoantibodies. *J. Autoimmun.* **62**, 81–92 (2015).
39. Y. Li, R. Chen, Q. Zhou, Z. Xu, C. Li, S. Wang, A. Mao, X. Zhang, W. He, H.-B. Shu, LSm14A is a processing body-associated sensor of viral nucleic acids that initiates cellular antiviral response in the early phase of viral infection. *Proc. Natl. Acad. Sci. U.S.A.* **109**, 11770–11775 (2012).
40. F. W. Fales, A potentiometric method for the determination of the iodine-binding capacity of glycogen. *Anal. Biochem.* **132**, 424–430 (1983).

Acknowledgments
Funding: This work was supported by the Natural Science Foundation of China (81861138002, 81722002, 31900654, and 31970839) and start-up funding from Huazhong University of Science and Technology. **Author contributions:** Y.J. drafted the initial manuscript. C.L. and B.Y. designed the study and reviewed and revised the manuscript. Y.J., X.D., D.K., and L.Y. performed the confocal and TIRF experiments. Y.J., P.J., N.L., J.C., and J.L. carried out the flow cytometry assay, ELISA, and Western blotting. Y.J., X.D., and L.Y. analyzed the data and generated figures. H.M., B.R., Q.G., W.Y., Z.L., P.K.M., Q.N., and J.S. assisted with the manuscript. All authors approved the final manuscript as submitted and agreed to be accountable for all aspects of the work. **Competing interests:** The authors declare that they have no competing interests. **Data and materials availability:** All data needed to evaluate the conclusions in the paper are present in the paper and/or the Supplementary Materials. Additional data related to this paper may be requested from the authors.

Submitted 8 May 2019
Accepted 24 January 2020
Published 22 April 2020
10.1126/sciadv.aax9455

Citation: Y. Jing, X. Dai, L. Yang, D. Kang, P. Jiang, N. Li, J. Cheng, J. Li, H. Miller, B. Ren, Q. Gong, W. Yin, Z. Liu, P. K. Mattila, Q. Ning, J. Sun, B. Yu, C. Liu, STING couples with PI3K to regulate actin reorganization during BCR activation. *Sci. Adv.* **6**, eaax9455 (2020).

Science Advances

STING couples with PI3K to regulate actin reorganization during BCR activation

Yukai Jing, Xin Dai, Lu Yang, Danqing Kang, Panpan Jiang, Na Li, Jiali Cheng, Jingwen Li, Heather Miller, Boxu Ren, Quan Gong, Wei Yin, Zheng Liu, Pieta K. Mattila, Qin Ning, Jinqiao Sun, Bing Yu and Chaohong Liu

Sci Adv **6** (17), eaax9455.
DOI: 10.1126/sciadv.aax9455